3-D Ego-Motion Estimation Using Multi-Channel FMCW Radar

Yuan, Sen; Zhu, Simin; Fioranelli, Francesco; Yarovoy, Alexander

DOI
10.1109/TRS.2023.3299180

Publication date
2023

Document Version
Final published version

Published in
IEEE Transactions on Radar Systems

3-D Ego-Motion Estimation Using Multi-Channel FMCW Radar

Sen Yuan, *Graduate Student Member, IEEE*, Simin Zhu, *Graduate Student Member, IEEE*, Francesco Fioranelli, *Senior Member, IEEE*, and Alexander G. Yarovoy, *Fellow, IEEE*

***Abstract*— The problem of estimating the 3D ego-motion velocity using multi-channel FMCW radar sensors has been studied. For the first time, the problem of ego-motion estimation is treated using radar raw signals. A robust algorithm using multi-channel FMCW radar sensors to instantly determine the complete 3D motion state of the ego-vehicle (i.e., translational speed and rotational speed) is proposed. The angle information of targets is extracted, and then their phase information from different times instances is used to determine vehicle ego-motion through an optimization process. Any pre-processing steps, such as clustering or clutter suppression, are not required. The performance of the algorithm is compared with the state-of-the-art algorithms based on real-world data, and superior performance has been demonstrated. The algorithm proposed can be easily integrated into radar signal processing pipelines for other tasks relevant to autonomous driving.**

***Index Terms*— Ego-motion estimation, multi-channel radar, velocity measurement, automotive application.**

I. Introduction

ROBUST ego-motion estimation plays an important role in various real-world applications, ranging from indoor robotics to automotive scenarios, and remains a challenging task. Various technologies and approaches have been developed to investigate robust solutions, aiming at more integrated, smaller, and power-efficient sensors.

These sensors include vision, laser, and classical navigation sensors like wheel-based odometry and inertial sensors. While extremely fast and high-resolution, lidar is sensitive to weather conditions, especially rain and fog [1]. Vision systems are versatile and cheap but easily impaired by scene changes, like poor lighting or the sudden presence of snow [2]. Both these sensors only yield dependable results for relatively short-range measurements. A typical GPS on its guarantees at best meter-level accuracy and may experience reception difficulties near obstructions and rely on external infrastructure [3]. Additionally, proprioceptive sensors, like wheel encoders and IMUs, suffer from significant drift among other detrimental effects [4], and may have systematic errors caused by kinematic imperfections, unequal wheel diameters or uncertainties about the exact wheelbase.

Manuscript received 25 January 2023; revised 16 May 2023; accepted 22 July 2023. Date of publication 26 July 2023; date of current version 15 August 2023. *(Corresponding author: Sen Yuan.)*

The authors are with the Microwave Sensing, Signals and Systems (MS3) Group, Delft University of Technology, 2628 CD Delft, The Netherlands (e-mail: s.yuan-3@tudelft.nl; s.zhu-2@tudelft.nl; f.fioranelli@tudelft.nl; a.yarovoy@tudelft.nl).

Digital Object Identifier 10.1109/TRS.2023.3299180

Radar technology has some unique advantages compared to other sensors, namely the accurate and direct measurements of the range, relative velocity, and angle of multiple targets, as well as a long-range coverage of more than 200 m even in challenging weather or light conditions [5]. Because of their high degree of integration and relatively low cost, radars operating in the 77 GHz mm-wave frequencies have become very popular [6], and nowadays, these sensors are considered key in autonomous driving [7]. With a large operational bandwidth, they can provide fine-range resolution. Doppler resolution is a function of chirp duration and the number of chirps used for the estimation, with better velocity resolution achieved by operating at higher frequency [8]. Angular resolution is contingent upon the antenna aperture and can be achieved by multi-channel radars, i.e., phased array [9], or multiple-input-multiple-output (MIMO) array techniques [10]. Both generate a real or virtual, typically uniform linear array (ULA) to improve angular information for imaging purposes.

When addressing the problem of ego-motion estimation, a current trend in automotive is information fusion from different sensors. Milli-RIO algorithm with data fusion coming from a single-chip low-cost radar and an inertial measurement unit sensor with an unscented Kalman filter and a Recurrent Neural Network (RNN) to estimate the six-degrees-of-freedom ego-motion of a moving radar is proposed in [11]. A comparison of the automotive SAR measurement of a static object and the representation of the static object from the digital map database to get an accurate localization is proposed in [12]. A millimeter-wave radar Simultaneous Localization and Mapping (SLAM) algorithm assisted by the Radar Cross Section (RCS) feature of the target and Inertial Measurement Unit (IMU) is suggested in [13]. A sliding window on radar measurements to extract Doppler velocity and IMU measurements to constrain the change in velocity between radar measurements, jointly estimating the 3D translational velocity, is suggested in [14]. Fusion of the radar's ego estimation results with monocular Visual Inertial Odometry or monocular Thermal Inertial Odometry to improve the robustness in challenging conditions is described in [15]. Finally, a fusion of the IMU data with radar data to correct the error in the estimation is proposed in [16].

Significant efforts have been made to use only information from multi-channel radar systems to perform ego-motion estimation. The state-of-the-art methods can be mainly divided into model-based and artificial intelligence (AI) approaches. Based on the vehicle's mechanical model, the sinusoidal

relation between the measured Doppler velocities and the azimuth angles is used in [17] to estimate the ego-motion. This work, which determined an ego-velocity vector of 2 degrees of freedom (DoF), was extended to the case of multiple distributed radars to deal with the full 2D vehicle motion state, i.e., 3 DoF [18]. A probabilistic model incorporating spatial registrations of radar scans was also proposed in [19]. That joint spatial and Doppler-based estimation operates without lever-arm offsets or motion assumptions but involves high computational costs. In subsequent research [20], the normal distribution transform (NDT) model was utilized for faster spatial alignment, and the complexity was further reduced by deriving a sparse probabilistic representation [21]. A hybrid approach [22] was proposed to decouple translational and rotational motion by combining benefits from scan matching and instantaneous approaches. The ego-motion velocities can also be calculated by the cross-correlation of different Tx-Rx pairs [23], [24]. A Gaussian Mixture Model for two consecutive point sets, achieving robust estimation results with a probabilistic strategy, is used in [25]. A new, unsupervised ego-velocity estimation method to allow a low-cost Doppler radar to obtain accurate ego-velocity estimation is presented in [26]. Ego-motion can also be generated using SLAM from radar data [27]. Although most of the newest algorithms for SLAM in ego-motion estimation [25], [28], [29] can provide a good performance by transferring the technique from Lidar or Odometry, they suffer from poor updating rate as they generally require a full frame to perform the ego-motion estimation. Moreover, the density of the radar point cloud is much sparser than a Lidar one, reducing the performance of these techniques. The AI-based algorithm [30] proposes an end-to-end (E2E) complex-valued neural network architecture using a complex-valued channel attention module that directly handles raw radar data to provide the ego-motion estimation. An ego-velocity prediction model using an LSTM network as a microscopic and non-parametric approach to applying to the various urban driving conditions is proposed in [31].

However, all the aforementioned algorithms for ego-motion estimation are based on radar point clouds, which are generated after several data processing steps. At least one coherent processing interval, i.e. one frame, is required to create such data clouds, which limits the possible update rate. Moreover, point clouds may not necessarily be coherent from frame to frame due to the scintillating scattering behaviour of extended targets at mm-wave frequencies, and their generation process can include artefacts coming from clutter and interference. Performing ego-motion estimation starting from the lower signal level (i.e., the radar base-band signal before range-doppler processing) can be beneficial in automotive scenarios. Firstly, the ego-motion estimation can be performed fast, within one frame or even from chirp to chirp. Secondly, using the algorithms implemented directly on the signal level, it will be easier to combine them with other high-resolution algorithms [32] or automotive SAR algorithms [33] to improve performances for other tasks, such as adaptive cruise control (ACC) [34], forward collision avoidance (FCA) [35], lane-change assistance [36], evasion assistance [37] or mapping generation [38]. To the best of our knowledge, only a few papers have been published to tackle ego-motion estimation from the radar raw signal. For example, the resolution autocorrelation in the range is used in [24] to estimate the ego-motion, but that algorithm operates at an intermediate frequency. The proposed method firstly estimates the targets' positions and then uses their phase information from different times instances to determine vehicle ego-motion through an optimization process.

The main contributions of this paper are listed as follows:

1) A novel 3D full ego-motion estimation algorithm working with radar raw signal at its input (i.e., the radar base-band signal before FFTs) is proposed by a two-step optimization.
2) It is demonstrated that using the algorithm proposed, 3 DoF ego-motion estimation can be performed on a smaller timescale than a frame and by using only one multi-channel radar.
3) A detailed analysis of the proposed method performance is provided based on numerical simulations with point targets and with realistic scenes reconstructed from the public *RadarScenes* dataset in [39].

The rest of the paper is organized as follows. In Section II, the signal model for a moving radar with 3 degrees of freedom is provided. The fundamentals of how to estimate the ego-motion velocity via the proposed optimization approach are demonstrated in Section III. The simulation results for ideal point targets and complex, realistic scenarios extracted from the *RadarScenes* dataset [39] are provided in Section IV. Finally, conclusions are drawn in Section V.

II. Signal Model

Frequency-modulated continuous wave (FMCW) radar with N_a antenna elements for azimuth estimation and N_e antenna elements for elevation estimation is considered here. Without losing generality, the omnidirectional antenna pattern is considered for the antenna elements. The FMCW chirp is characterized by its chirp duration T_c and pulse repetition interval (PRI) T. A normalized single chirp signal with bandwidth B has the form:

$$s_0(t) = \begin{cases} e^{j2\pi(f_0 t + 0.5\mu t^2)} & t \in [0, T_c] \\ s_{\text{settle}}(t) & t \in [T_c, T] \end{cases} \tag{1}$$

where f_0 denotes the starting frequency of the chirp, $\mu = \frac{B}{T_c}$ denotes the frequency modulation rate, and $s_{\text{settle}}(t)$ indicates the signal during the settle time. This is the time when radar chirps are reset to the starting frequency to allow the hardware circuitry to settle.

The periodic transmitted signal is decomposed into fast-time domain t' and chirp number domain $l = \lfloor \frac{t}{T} \rfloor$ as $t' = t - lT$, with $t' \in [0, T_c]$, where $l = 0, 1, 2, \ldots, L_d - 1$, and L_d is the total number of the chirps in one snapshot or frame.

Then the periodically transmitted chirp signal can be expressed as:

$$s(t) = s(t' + lT) = s(l, t') = s_0(t') \tag{2}$$

The round trip delay of the reflected signal from a scatterer for the i-th virtual antenna is:

$$\tau_{\mathbf{o}}(l,t') = \frac{2\big(D_{\mathbf{o}}(t'+lT)+v\big(t'+lT\big)\big)}{c} \approx \gamma_{\mathbf{o}} + \frac{2v(t'+lT)}{c} \tag{3}$$

where c is the speed of light, $D_{\mathbf{o}}(t'+lT)$ is the distance between the target $\mathbf{o}$ and the radar at time $(t'+lT)$, and v is the radial velocity between the radar and scatter.

The corresponding received signal can be written as:

$$\begin{aligned} r_{(\mathbf{o},i,j)}(l,t') &= \alpha e^{j\phi_{\mathbf{o},i,j}} s(t'+lT-\tau_{\mathbf{o}}(l,t')) \\ &= \alpha e^{j\phi_{\mathbf{o},i,j}} e^{j2\pi\Phi_{\mathbf{o}}(l,t')} \\ with\ t' &\in [\gamma_{\mathbf{o}}, T_c] \end{aligned} \tag{4}$$

where α is the constant complex coefficient of the scatterer, and $e^{j\phi_{\mathbf{o},i,j}}$ denotes the phase delay of the scatterer $\mathbf{o}$ at the i,j-th virtual element. According to (2), the term $\Phi_{\mathbf{o}}(l,t')$ has the form:

$$\begin{aligned} &\Phi_{\mathbf{o}}(l,t') = f_0(t'-\tau_{\mathbf{o}}(l,t')) + 0.5\mu(t'-\tau_{\mathbf{o}}(l,t')^2), \\ &with\ t' \in [\gamma_{\mathbf{o}}, T_c] \end{aligned} \tag{5}$$

The phase delay of the i,j-th antenna elements counted in the 2-D linear array and relative to the 1st antenna element, i.e., the reference antenna element, is obtained by:

$$\phi_{\mathbf{o},i,j}(l) \approx 2\pi f_0\left(\frac{d_i}{c}\sin\theta_{\mathbf{o}}(\mathrm{l})\cos\phi_{\mathbf{o}}(l) + \frac{d_j}{c}\sin\phi_{\mathbf{o}}(\mathrm{l})\right) \tag{6}$$

where d_i and d_j are the reference distances between the 1st antenna element in azimuth and elevation direction, respectively. The $\theta_{\mathbf{o}}(l)$ and $\phi_{\mathbf{o}}(l)$ are the azimuth angle and elevation angle of the $\mathbf{o}$-th scatterer at slow time l, respectively. For the automotive radar's case, where the MIMO technology is the major trend in current applications [40], the equation (6) needs to be changed to:

$$\phi_{\mathbf{o},i,j}(l) \approx 2\pi f_0\left(i\frac{d}{c}\sin\theta_{\mathbf{o}}(\mathrm{l})\cos\phi_{\mathbf{o}}(l) + j\frac{d}{c}\sin\phi_{\mathbf{o}}(\mathrm{l})\right) \tag{7}$$

Here, we assume that the rotation during the fast time has no influence as the fast time has a very short duration. Also, the velocity of different antennas due to the rotation will not influence the Doppler velocity (otherwise, the antennas will lose their coherency), and these differences are negligible because the rotating radial distance between them is only half wavelength. Hence, the change in angle is due to the vehicle's rotation in pitch, roll, and yaw directions, $[\Theta_p, \Theta_r, \Theta_y]$, which can be calculated at a given time as the following:

$$\begin{aligned} &A_{xyz}(\Theta_p,\Theta_r,\Theta_y) \\ &= A_x(\Theta_p)A_y(\Theta_r)A_z(\Theta_y) \\ &= \begin{bmatrix} \cos(\Theta_y) & -\sin(\Theta_y) & 0 \\ \sin(\Theta_y) & \cos(\Theta_y) & 0 \\ 0 & 0 & 1 \end{bmatrix} \begin{bmatrix} \cos(\Theta_r) & 0 & \sin(\Theta_r) \\ 0 & 1 & 0 \\ -\sin(\Theta_r) & 0 & \cos(\Theta_r) \end{bmatrix} \\ &\quad \times \begin{bmatrix} 1 & 0 & 0 \\ 0 & \cos(\Theta_p) & -\sin(\Theta_p) \\ 0 & \sin(\Theta_p) & \cos(\Theta_p) \end{bmatrix} \end{aligned} \tag{8}$$

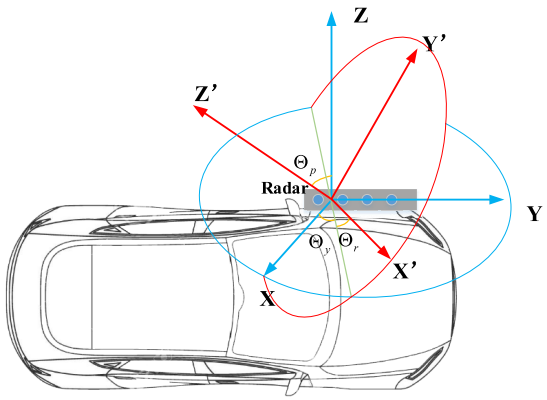

Fig. 1. The geometry of the rotation of the radar mounted to the side of a vehicle.

The geometry of the radar mounted on the vehicle is shown in Fig. 1. A side-looking radar is considered as the paper focuses on solving the ego-velocity estimation of the radar platform, which can then be linearly connected to the velocity of the vehicle on which the radar is mounted. So the position in the coordinates of the target $\mathbf{o}$ can be calculated for the radar with rotation speed $[\omega_p, \omega_r, \omega_y]$ as (9):

$$\begin{aligned} &\begin{bmatrix} R_{\mathbf{o}}\cos(\theta_{\mathbf{o}}(l))\cos(\phi_{\mathbf{o}}(l)) \\ R_{\mathbf{o}}\sin(\theta_{\mathbf{o}}(l))\cos(\phi_{\mathbf{o}}(l)) \\ R_{\mathbf{o}}\sin(\phi_{\mathbf{o}}(l)) \end{bmatrix} \\ &= A_{xyz}(\omega_p l, \omega_r l, \omega_y l) \begin{bmatrix} R_{\mathbf{o}}\cos(\theta_{\mathbf{o}}(0))\cos(\phi_{\mathbf{o}}(0)) \\ R_{\mathbf{o}}\sin(\theta_{\mathbf{o}}(0))\cos(\phi_{\mathbf{o}}(0)) \\ R_{\mathbf{o}}\sin(\phi_{\mathbf{o}}(0)) \end{bmatrix} \end{aligned} \tag{9}$$

The received signal is then correlated with the conjugate copy of the transmitted signal to derive the de-chirped signal of the $\mathbf{o}$-th scatterer received by the i,j-th element. This can be written as in (10), where for simplicity, the complex coefficient of the de-chirped signal is still indicated:

$$\begin{aligned} z_{(\mathbf{o},i,j)}(l,t') &= r_{(\mathbf{o},i,j)}(l,t') \times s^*(l,t') \\ &= \alpha_{\mathbf{o}} \exp[j\phi_{\mathbf{o},i,j}(l)] \\ &\quad \times \exp[-j2\pi(f_0\frac{2v}{c}Tl + \mu\gamma_{\mathbf{o}}t')] \\ &\quad \times \exp[-j2\pi\mu\frac{2v}{c}Tlt'] \end{aligned} \tag{10}$$

After the de-chirping, the data in (10) is sampled with respect to fast-time with frequency f_s and the discretized data $\hat{z}_{\mathbf{o}}^{i,j}$ in the time domain is obtained as

$$\hat{z}_{\mathbf{o}}^{i,j}(l,b) \approx \alpha_{\mathbf{o}} \exp[j\phi_{\mathbf{o},i,j}(l) - j2\pi(f_{d,\mathbf{o}}Tl + \mu\gamma_{\mathbf{o}}\frac{b}{f_s})] \tag{11}$$

where $f_{d,\mathbf{o}} = \frac{2v_{\mathbf{o}}f_0}{c}$ represents the Doppler frequency of the $\mathbf{o}$-th scatter. The coupling terms between slow time and fast time can be neglected because the automotive radar is typically working with the narrow bandwidth assumption.

When there are N_s scatterer points in the field of view, the signal would be as follows based on the superposition of the contributions of each scatterer:

$$\hat{z}^{i,j}(l,b) = \sum_{\mathbf{o}}^{N_s} \hat{z}_{\mathbf{o}}^{i,j}(l,b) \tag{12}$$

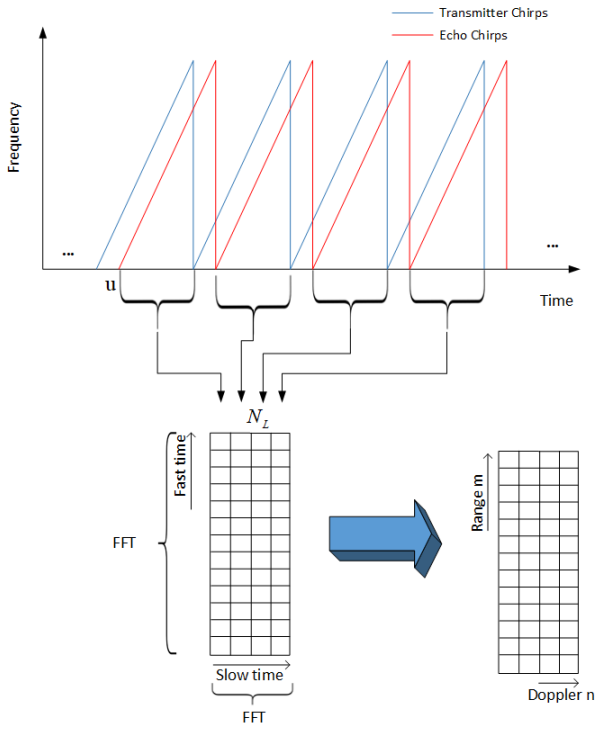

Fig. 2. The generation of Range-Doppler Spectra (RDS), where u is the index controlling the starting time of the group of chirps within one frame that is selected for further processing.

III. Proposed Method

In this section, the proposed method for ego-motion estimation is presented.

A. Steps for the Proposed Ego-Motion Estimation

For each antenna, one can obtain the range–Doppler spectrum (RDS) by performing the 2-dimensional FFT (2D FFT) of the de-chirped signal in a fast and slow time.

For the signal received by one antenna, it is important to note that a group of chirps in the whole frame will be chosen for further processing, i.e., $\hat{z}(u : u + N_L - 1, k)$, with $u \in \mathbb{N}, u + N_L < L_d$. u is the starting slow time index for the selected group of chirps, as shown in Fig. 2. Compared to alternative point cloud-based methods for ego-velocity estimation, the updating rate of this and the following steps can be significantly improved from frame to chirp rate by allowing overlap between the selected groups of chirps. After 2D FFT, the signal for the selected group of chirps in (12) will become:

$$\begin{aligned}\hat{z}^{i,j}(m,n,u) = \sum_{\mathbf{o}}^{k} \alpha_{\mathbf{o}} \pi^2 T_c f_s N_L \operatorname{sinc}\left(\frac{(mT_c f_s + \mu\gamma_{\mathbf{o}} T_c)}{2}\right) \\ \times \operatorname{sinc}\left(\frac{(n + f_{d,\mathbf{o}} T) N_L}{2}\right) \times \exp[j\Phi_{\mathbf{o},i,j}(l)] \\ \times \exp[-j\pi((mT_c f_s + \mu\gamma_{\mathbf{o}} T_c) \\ + (n + f_{d,\mathbf{o}} T)(2u + N_L))] \end{aligned} \tag{13}$$

where m and n are the indices of the frequency in range and Doppler domain, respectively. Because of the sinc function in the expression, the amplitude peak will change according to the Doppler velocity and range of targets, which is at the basis of the subsequent detection processing.

Range and Doppler detection can be performed using thresholding-based methods applied to the 2D RDS, such as the constant false alarm rate detector (CFAR) [41]. There are many different versions of CFAR, but the core theory is to estimate the background power and achieve a constant false alarm rate in detection. Also, AI-based detectors have been proposed recently, but they are focused on a specific type of target's detection, e.g., ships [42] or underground targets [43]. In this work, a conventional cell-averaging CFAR algorithm is applied [44]. The radar is installed on the side of the vehicle. This can effectively avoid the Doppler ambiguity problem encountered in forward-looking radar, and help distinguish the targets' contribution over the whole Doppler spectrum. Via the 2D FFT, the targets can then be separated in the range and Doppler domains. The detections are based on the amplitude information of the RDSs, which are independent of the antenna and the starting slow time index, as in (13). It should also be noted that each detected bin may contain the contribution of multiple physical targets or scatter points, but these can be regarded by the algorithm as a single "synthetic target" for a given detected bin. In other words, there is no explicit assumption that one detected range-Doppler bin would correspond to one specific physical target. It is also assumed that this will not change much in the short duration of one CPI/frame over which the algorithm operates.

After CFAR detection, N_k range-Doppler cells are obtained for every RDS, denoted by $[(m_1, n_1); (m_2, n_2); \ldots; (m_{N_k}, n_{N_k})]$. These cells will be used to select the corresponding vectors along the antenna/channel dimension of the radar cube for subsequent processing. With FFTs and detections, the proposed ego-motion estimation approach uses as its input raw data from different chirps of the radar cube, rather than discrete points from a point cloud after detection. In the following subsections, the estimation of the rotational and translational velocities are presented.

1) Rotational Motion: The phase differences between different antennas for the detected range-Doppler cell will only depend on the angular information of those targets belonging to this cell, i.e., their position in terms of elevation angle and azimuth angle in (7). From this, we can extract the angle information of these detected cells, i.e. the angle information of this synthetic target.

By stacking all the RDS at a time u for the detected (m_k, n_k) range-Doppler indices, the target data for each cell is written in the matrix format $\overrightarrow{Z}(m_k, n_k, u)$ as:

$$\begin{aligned}&\overrightarrow{Z}(m_k, n_k, u) \\ &= \begin{bmatrix} \hat{z}^{1,1}(m_k, n_k, u) & \cdots & \hat{z}^{1,N_e}(m_k, n_k, u) \\ \cdots & \hat{z}^{i,j}(m_k, n_k, u) & \cdots \\ \hat{z}^{N_a,1}(m_k, n_k, u) & \cdots & \hat{z}^{N_a,N_e}(m_k, n_k, u)) \end{bmatrix}\end{aligned} \tag{14}$$

Here, the k-th detected RDS is assumed to belong to the k-th 'synthetic target', whose phase information will follow:

$$\exp[j\Phi_{\mathbf{k},i,j}(l)] = \sum_{k_i=1}^{k_n} \exp[j\Phi_{\mathbf{k}_i,i,j}(l)] \tag{15}$$

where k_i the index of the targets in k-th bin, k_n is the total number of targets in k-th bin. As discussed, here a 'synthetic target' occupying one bin does not necessarily relate to a single physical object.

We then take this target as an example, $Z^{i,j}(m_k, n_k, u) \in \mathbb{C}^{N_a \times N_e}$, where i, j denote the index of the antennas in azimuth and elevation, respectively, and N_a, N_e are the total number of antennas in azimuth and elevation. By applying equation (13), each element $\hat{z}^{i,j}(m_k, n_k, u)$ will be written as:

$$\hat{z}^{i,j}(m_k, n_k, u) = \beta \hat{z}^{1,1}(m_k, n_k, u) \exp[j\phi_{\mathbf{k},i,j}(u)] \tag{16}$$

where β is the complex coefficient containing the information about the amplitudes, and $\hat{z}^{1,1}(m_k, n_k, u)$ is the received signal from the reference antenna element.

To estimate the rotational motion, two RDSs starting from different slow time values are needed, u_0 and u_1. The range and Doppler indices for a detected target at time u_0 will also be used for the next RDS at time u_1, as it is assumed that they remain the same during a few chirps. These can be written in the matrix format as $\overrightarrow{Z}(m_k, n_k, u_0)$ and $\overrightarrow{Z}(m_k, n_k, u_1)$.

From the phase differences in (16), the angle of the 'synthetic target' at a time u_1 is derived as discussed later in Section III-B, i.e. $\overrightarrow{Z}(m_k, n_k, u_0) \Rightarrow [\hat{\theta}_{\mathbf{k}}(u_0), \hat{\phi}_{\mathbf{k}}(u_0)]$ and $\overrightarrow{Z}(m_k, n_k, u_1) \Rightarrow [\hat{\theta}_{\mathbf{k}}(u_1), \hat{\phi}_{\mathbf{k}}(u_1)]$.

With radar, the targets' range information $\hat{r_{\mathbf{k}}}(u)$ can be easily estimated. Then for k detected targets, a matrix $\overrightarrow{T_c}(u) \in \mathbb{C}^{N_k \times 3}$ can be formed, which contains their different position information, namely range, azimuth, elevation:

$$\overrightarrow{T_c}(u) = \begin{bmatrix} \hat{r_{\mathbf{1}}}(u) & \dots & \hat{r_{\mathbf{k}}}(u) \\ \hat{\theta_{\mathbf{1}}}(u) & \dots & \hat{\theta_{\mathbf{k}}}(u) \\ \hat{\phi_{\mathbf{1}}}(u) & \dots & \hat{\phi_{\mathbf{k}}}(u) \end{bmatrix} \tag{17}$$

At this stage, three operations are implemented to estimate the rotational velocities: first, the projection to Cartesian coordinates; second, Kabsch algorithm [45], [46] as shown in Algorithm. 1 to estimate the rotation matrix; finally, the estimation of the rotational velocities based on the rotation matrix. These steps are summarized in Section III-C.

2) Translational Motion: The phase differences between different starting slow time indices for the detected cell will be dependent on the 'synthetic target' Doppler information, which can be seen in (13). To estimate the translational motion from these phase differences, the same process can be applied as the one performed for the angle extraction in the aforementioned rotation estimation.

The Doppler velocity V_d only contains the components of the vehicle and the targets' relative speed in the radial direction. Here, the majority of the Doppler components come from the radar's speed. This is true especially for side-looking radars, as most targets in the radar field of view are static, like landmarks, road curbs, and buildings. Only the car's movement is considered for simplicity in this derivation. Also, the detected Doppler velocity is already combined with all the Doppler components from every target in the given cell. The ego-motion estimation of the radar can be derived from the phase differences.

Once again, let us take the detected $\mathbf{k}$-th target as an example. The radar is moving with velocity $v_r(u) = [v_{rx}(u), v_{ry}(u), v_{rz}(u)]$. Assuming that during the short period $u_1 - u_0$ the relative speed between targets and radar remains constant. Also, the targets within one detected bin will be at the same position. The phase difference $\Gamma(\mathbf{k}, u_1, u_0)$ can be written as:

$$\Gamma(\mathbf{k}, u_1, u_0) = 4\pi \frac{dr_{\mathbf{k}} f_0}{c} T \tag{18}$$

$$\begin{aligned} dr_{\mathbf{k}} = V_d * (u_1 - u_0) &= v_{rx}(u_0) * (u_1 - u_0) \cos\theta_{\mathbf{k}} \cos\phi_{\mathbf{k}} \\ &+ v_{ry}(u_0) * (u_1 - u_0) \sin\theta_{\mathbf{k}} \cos\phi_{\mathbf{k}} \\ &+ v_{rz}(u_0) * (u_1 - u_0) \sin\phi_{\mathbf{k}} \end{aligned} \tag{19}$$

By stacking all the detected range-Doppler cells at a certain time u, the matrix for translational motion can be formed as $\overrightarrow{T_t}(u) \in \mathbb{C}^{N_a * N_e \times N_k}$:

$$\overrightarrow{T_t}(u) = \begin{bmatrix} \hat{z}^{1,1}(m_1, n_1, u) & \dots & \hat{z}^{1,1}(m_1, n_1, u) \\ \dots & \dots & \dots \\ \hat{z}^{N_a,N_e}(m_{N_k}, n_{N_k}, u) & \dots & \hat{z}^{N_a,N_e}(m_{N_k}, n_{N_k}, u) \end{bmatrix} \tag{20}$$

with the two matrices $\overrightarrow{T_t}(u_0)$, $\overrightarrow{T_t}(u_1)$ related to time u_0, u_1. An element of these matrices can be written as in (21):

$$Z^{i,j}(m_k, n_k, u_1) = \beta Z^{i,j}(m_k, n_k, u_0) \exp[j\Gamma(\mathbf{k}, u_1, u_0)] \tag{21}$$

From the phase differences in (21), the translational movement of the radar is derived as discussed in the following Section III-B, i.e. $[\overrightarrow{T_t}(u_0), \overrightarrow{T_t}(u_1) \Rightarrow [\hat{v_{rx}}, \hat{v_{ry}}, \hat{v_{rz}}]$.

B. Details of the Optimization Approach

Both equations (21) and (16) have the same format, only with different phase information. Here, the problem can be formulated as to how to estimate the desired parameters, i.e., the angular position of the target and the translational velocity, from the phase information in the presence of noise.

From the equation (16), the measured data in a matrix form $X \in \mathbb{C}^{N_a \times N_e}$ can be obtained:

$$X = \frac{Z^{i,j}(m_k, n_k, u)}{Z^{1,1}(m_k, n_k, u)} + N_x \tag{22}$$

where $N_x \in \mathbb{C}^{N_a \times N_e}$ is the noise matrix.

The signal model $Y \in \mathbb{C}^{N_a \times N_e}$ was designed for subsequent optimization as:

$$Y(\hat{\theta_{\mathbf{k}}}, \hat{\phi_{\mathbf{k}}}) = \exp\left(j2\pi f_0 \left(\frac{d_i}{c} \sin\hat{\theta_{\mathbf{k}}} \cos\hat{\phi_{\mathbf{k}}} + \frac{d_j}{c} \sin\hat{\phi_{\mathbf{k}}}\right)\right) \tag{23}$$

where $i \in [0, N_a]$ and $j \in [0, N_e]$ are the indices of the matrix, respectively, and the d_i and d_j have been defined in (7).

The problem then becomes an optimization problem, with the objective defined as:

$$\arg\min_{\hat{\theta_{\mathbf{k}}}, \hat{\phi_{\mathbf{k}}}} f(\hat{\theta_{\mathbf{k}}}, \hat{\phi_{\mathbf{k}}}) \tag{24}$$

where $f(\hat{\theta_{\mathbf{k}}}, \hat{\phi_{\mathbf{k}}}) = [Y - X]^H [Y - X]$, with $X, Y \in \mathbb{C}^{N_a \times N_e}$.

Different optimization algorithms can be used here, e.g., genetic algorithm [47] or simulated annealing [48]. Pattern search [49] is used for solving this optimization problem.

In this way, one can obtain the estimated $\hat{\theta}_{\mathbf{k}}$ and $\hat{\phi}_{\mathbf{k}}$ for different detected targets. The advantage of this method is that it can be extremely simple to formulate and implement, as it does not require an explicit estimate of the derivative of the function or Taylor's series. Furthermore, it is globally convergent [50].

Similarly, from the equation (21), the measured data can be obtained and written as a matrix $P \in \mathbb{C}^{N_k \times N_e N_a}$

$$P = \frac{Z^{i,j}(m_k, n_k, u_1)}{Z^{i,j}(m_k, n_k, u_0)} + N_p \tag{25}$$

where $N_p \in \mathbb{C}^{N_k \times N_e N_a}$ is the noise matrix.

We can design the signal model $Q \in \mathbb{C}^{N_k \times N_e N_a}$ as:

$$\begin{aligned} Q(\hat{v_{rx}}, \hat{v_{ry}}, \hat{v_{rz}}) &= \exp(j4\pi T(v_{rx}(u_0) * (u_1 - u_0)\cos\hat{\theta}_{\mathbf{k}}\cos\hat{\phi}_{\mathbf{k}} \\ &+ v_{ry}(u_0) * (u_1 - u_0)\sin\hat{\theta}_{\mathbf{k}}\cos\hat{\phi}_{\mathbf{k}} \\ &+ v_{rz}(u_0) * (u_1 - u_0)\sin\hat{\phi}_{\mathbf{k}})f_0/c) \\ &\times ones(1, N_e N_a) \end{aligned} \tag{26}$$

where $\hat{\theta}_{\mathbf{k}}$ and $\hat{\phi}_{\mathbf{k}}$ are the estimated azimuth and elevation angle of detected targets in (24).

This problem becomes another optimization problem, with the objective defined as:

$$\arg \min_{\hat{v_{rx}}, \hat{v_{ry}}, \hat{v_{rz}}} f(\hat{v_{rx}}, \hat{v_{ry}}, \hat{v_{rz}}) \tag{27}$$

where $f(\hat{v_{rx}}, \hat{v_{ry}}, \hat{v_{rz}}) = [Q - P]^H[Q - P]$, with $Q, P \in \mathbb{C}^{N_k \times N_e N_a}$.

This problem is also solved with pattern search [49] to estimate $\hat{v_{rx}}, \hat{v_{ry}}, \hat{v_{rz}}$.

The proposed method mainly depends on the two optimization steps. Hence, the computation complexity depends on these two steps, i.e., on the number of iterations required for each optimization. The optimization in (24) is implemented for each detected range-Doppler cell to obtain all the targets' angle information. Thus, the computation complexity of the first optimization step mainly comes from the number of range-Doppler cells with detected targets. The number of iterations depends on the convergence threshold set; specifically, in this paper an average of 80 times per optimization was performed.

C. Summary of the Proposed Algorithm

Based on the fundamentals described in the previous subsections, ego-motion estimation can be performed by optimizations starting from the received radar signal. To summarize, the steps of the proposed approach are described as follows.

Step 1: Detection Based on the RDS:

After 2D FFT on fast time and slow time, the radar raw signal will be converted into RDS data. Using 2D cell-averaging CFAR detection [44], the detected targets' indices in range and Doppler domain will be obtained.

Step 2: Optimization of Two Consecutive RDS's Angle Information:

By stacking all the RDS starting from time u_0 for each detected targets, as in equation (16), the optimization can be performed as described in (24) to obtain the azimuth $\hat{\theta}_{u_1}$ and elevation angle $\hat{\phi}_{u_1}$ for the detected targets at time u_1.

Step 3: Estimation of the Rotational Speed:

For the time u_1, we can obtain the matrix $\overrightarrow{T_c}(u)$ containing ranges, azimuths angles and elevation angles for each detected target as shown in (17). By performing the projection (28), the locations of the targets are converted into Cartesian coordinates system. The matrix in (17) can be converted as $\overrightarrow{T_p}(u)$. The locations of all the detected targets at two different times are stacked separately in the same order to form two matrices $\overrightarrow{T_p}(u_0)$ and $\overrightarrow{T_p}(u_1)$.

$$\begin{bmatrix} \hat{x_{\mathbf{k}}}(u) \\ \hat{y_{\mathbf{k}}}(u) \\ \hat{z_{\mathbf{k}}}(u) \end{bmatrix} = \begin{bmatrix} \hat{r_{\mathbf{k}}}(u)\cos(\hat{\theta}_{\mathbf{k}}(u))\cos(\hat{\phi}_{\mathbf{k}}(u)) \\ \hat{r_{\mathbf{k}}}(u)\sin(\hat{\theta}_{\mathbf{k}}(u))\cos(\hat{\phi}_{\mathbf{k}}(u)) \\ \hat{r_{\mathbf{k}}}(u)\sin(\hat{\phi}_{\mathbf{k}}(u)) \end{bmatrix} \tag{28}$$

Kabsch algorithm [45], [46] as shown in Algorithm. 1 is then used here to obtain the rotation matrix $R \in \mathbb{C}^{3\times3}$ between two datasets.

Algorithm 1 Kabsch algorithm

Get the position matrix of point clouds from two datasets $\overrightarrow{T_p}(u_0)$ and $\overrightarrow{T_p}(u_1)$, where p_i and p'_i are the coordinate values of each point, respectively.

Calculate the centroid of each point cloud:

$p = \frac{1}{n}\sum_{i=1}^{N_k} p_i$

$p' = \frac{1}{n}\sum_{i=1}^{N_k} p'_i$

The displacement vector of each point relative to the centroid is defined as:

$q_i = p_i - p$

$q'_i = p'_i - p'$

Calculate the covariance matrix of those points:

$H = \sum_{i=1}^{N_k} q q'^T$

Perform the SVD decomposition:

$H = U \wedge V^T$

$R = V U^T$

The rotational matrix R can be obtained.

Then the rotation angle for each axis can be calculated by the elements in the obtained rotational matrix R:

$$\begin{bmatrix} \Theta_p \\ \Theta_r \\ \Theta_y \end{bmatrix} = \begin{bmatrix} \tan^{-1}(\frac{R_{3,2}}{R_{3,3}}) \\ \tan^{-1}(\frac{-R_{3,1}}{\sqrt{R_{1,1}^2 + R_{2,1}^2}}) \\ \tan^{-1}(\frac{R_{2,1}}{R_{1,1}}) \end{bmatrix} \tag{29}$$

Hence, each component of the rotational speed will be:

$$\begin{bmatrix} \omega_p \\ \omega_r \\ \omega_y \end{bmatrix} = \begin{bmatrix} \frac{\Theta_p}{T(u_1 - u_0)} \\ \frac{\Theta_r}{T(u_1 - u_0)} \\ \frac{\Theta_y}{T(u_1 - u_0)} \end{bmatrix} \tag{30}$$

where T is the chirp duration time.

Step 4: Estimation of the Translational Speed:

Start by stacking the two antenna elements vector starting from time u_0 and time u_1 for each detected target (m_{Nk}, n_{Nk}), as in equation (21). The optimization can then be performed as described in (27) to obtain the translational speed of the radar $\hat{v_{rx}}, \hat{v_{ry}}, \hat{v_{rz}}$.

The entire proposed algorithm is summarized in the pseudocode shown in Algorithm 2, and the corresponding block diagram was drawn in Fig.3.

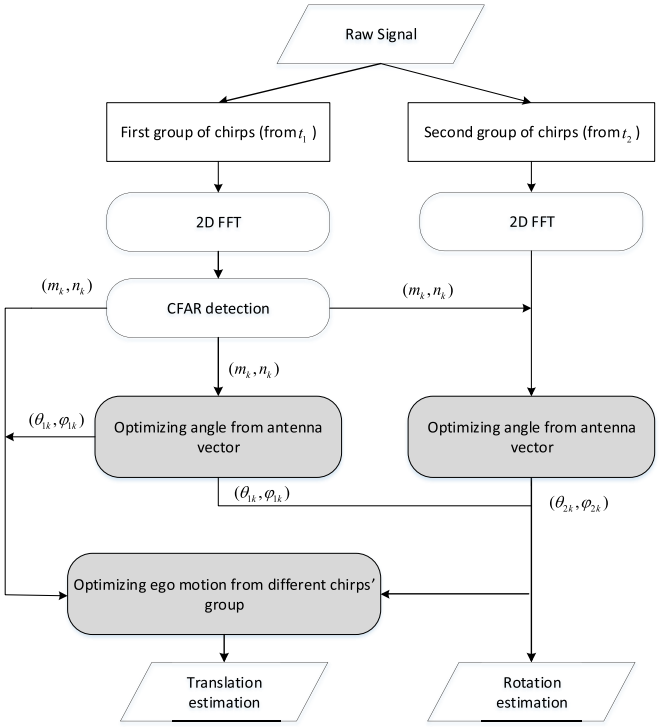

Fig. 3. The block diagram of the proposed method, where after obtaining raw radar data, a 2D FFT is performed for a different group of chirps with different starting times t_1 and t_2. This is followed by CFAR detection and proposed optimization process to finally obtain the ego-motion estimation, i.e. the estimation of the rotation and translation velocity components.

D. Limitations

A detailed discussion of the results is shown in the following section, where some limitations of the current formulation of the algorithm are reported.

On one hand, it is noted the dependence of the ego-velocity estimation quality on the number of detected targets in the scene. These cannot be distributed in every range and Doppler cell, which means that too many targets will degrade the performances of the proposed method (see Table III in the following section). On the other hand, too few targets will lead to higher errors in the ego-motion estimation because of the residual uncertainty.

Also, the second optimization step relies on the Doppler information. Thus, the maximum estimated velocity for the algorithm should be less than the maximum unambiguous velocity V_{max}. Current generation of MIMO automotive radar applies often Time Division Multiplexing (TDM) to achieve orthogonal transmit signals. Thus, the maximum unambiguous velocity can be expressed as:

$$V_{max} = \frac{\lambda}{4T_c * N_{ta} * N_{te}} \tag{31}$$

where N_{ta} and N_{te} are the number of transmitters for azimuth and elevation directions, respectively. The result with the radar parameters used in the simulation and listed in Table I is approximately 80 km/h. It should also be noted that working with Code Division Multiplexing or Frequency Division Multiplexing rather than TDM means that the unambiguous velocity range can be further extended.

Algorithm 2 Proposed method of this paper

Perform 2D FFT on fast time and slow time for the groups of chirps starting from time u_0 and u_1 in a frame to obtain the RDSs $\hat{z}^{i,j}(m, n, u_0)$ and $\hat{z}^{i,j}(m, n, u_1)$ as in (12)
Perform 2D cell-averaging CFAR detection [44] on RDS $\hat{z}^{1,1}(m, n, u_0)$ to get the targets' range-Doppler cells $[(m_1, n_1); (m_2, n_2); \ldots; (m_{Nk}, n_{Nk})]$.
Stack all the detected RDSs at time u_0 and u_1 to get $\overrightarrow{Z}(m_k, n_k, u_0)$ and $\overrightarrow{Z}(m_k, n_k, u_1)$
Form the measure data X as in (22) and build the model data Y as in (23).
Use pattern search for solving the optimization problem (24) to estimate the azimuth and elevation angle $[\hat{\theta}_{\mathbf{k}}(u_0), \hat{\phi}_{\mathbf{k}}(u_0)]$ and $[\hat{\theta}_{\mathbf{k}}(u_1), \hat{\phi}_{\mathbf{k}}(u_1)]$.
Extract the range information $\hat{r_{\mathbf{o}_1}}(u)$ from the detection of the range-Doppler matrix.
Project the detected targets from polar coordinates to the cartesian coordinates, as in (28).
Perform the Kabsch algorithm as shown in Algorithm 1.
Calculate the rotational angle of each axis as in (29).
Calculate the rotational speed as in (30).
Stack all the detected RDSs at time, u_0 and u_1 to get $\overrightarrow{T_t}(u_0)$ and $\overrightarrow{T_t}(u_1)$ as in (20)
Form the measure data P as in (25), and build the model data Q as in (26).
Use pattern search for solving the optimization problem (27) to estimate the translational speed, i.e. $[\hat{v_{rx}}, \hat{v_{ry}}, \hat{v_{rz}}]$
The 3D ego estimation can finally be obtained.

TABLE I
THE RADAR PARAMETERS FOR THE VERIFICATION OF THE METHOD

Parameters	Value
Central Frequency (GHz)	77
Slope (MHz/us)	62.5
Sampling Rate (Msps)	32
Bandwidth (GHz)	1
PRI (us)	20
Number of chirps per frame	256

IV. RESULTS AND DISCUSSION

To show the effectiveness of the proposed method, several results based on groups of simulated point targets and realistic scenarios derived from the automotive radar datasets *RadarScenes* [39] are presented in this section.

A. Simulated Point Targets

We used a simulated 8×8 2D uniform linear array on the side-looking radar to evaluate the performance of the approach. The distances between different antennas are constant, $\frac{\lambda}{2}$, to avoid ambiguity. The radar parameters are listed in Table I.

Fifty random targets are generated in the radar field of view, i.e. at random range values in the interval $[0, 35m]$, elevation in the interval $[0, 60°]$, and azimuth in the interval $[-30°, 30°]$ with random RCS. The vehicle is moving with random speed selected from a uniform distribution in all three coordinates where $V_x = \mathcal{U}(-10.8\ km/h, 10.8\ km/h)$, $V_y = \mathcal{U}(32.4\ km/h, 50.4\ km/h) = \mathcal{U}(9m/s, 14m/s)$, $V_z = \mathcal{U}(-10.8\ km/h, 10.8\ km/h) = \mathcal{U}(-3m/s, 3m/s)$,

TABLE II
THE EVALUATION RESULTS FOR THE TRANSLATIONAL EGO-VELOCITY ESTIMATION USING SIMULATED POINT TARGETS

Velocity	Parameter	Proposed	Modified DOA
X direction	Mean (mm/s)	1.5	46
	Variance (10^{-4})	0.088	34.0
Y direction	Mean (mm/s)	4.0	51.2
	Variance (10^{-4})	0.573	43.0
Z direction	Mean (mm/s)	4.2	64.8
	Variance (10^{-4})	0.581	67.0

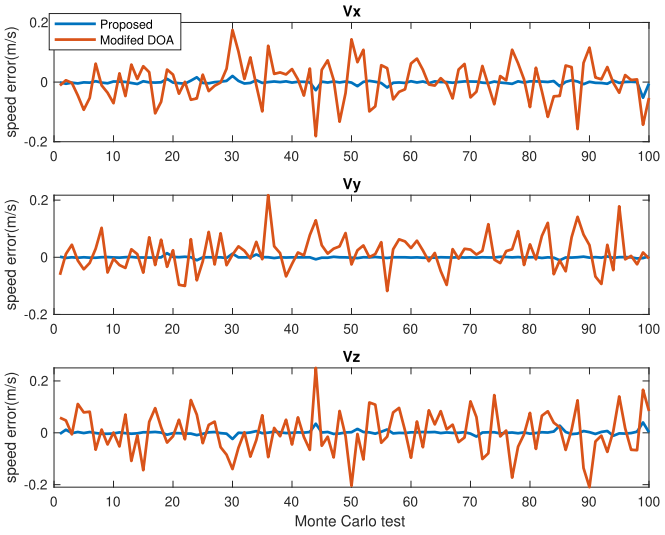

Fig. 4. Performance comparison in terms of velocity error [m/s] for 3D translational velocity estimation for simulated targets. (a) Velocity in the X direction. (b) Velocity in the Y direction. (c) Velocity in the Z direction. The proposed method (blue) is compared with the modification of the method (red) in [17].

and $w_p, w_r, w_y = \mathcal{U}(-15°/s, 15°/s)$. The corresponding value of the three translational velocity components in m/s is $V_x = \mathcal{U}(-3m/s, 3m/s)$, $V_y = \mathcal{U}(9m/s, 14m/s)$, $V_z = \mathcal{U}(-3m/s, 3m/s)$. All the targets are set to be static for this first simulation.

As this work is the first to implement 3 DoF ego-motion estimation using low-level data from only one radar to provide a state-of-the-art reference, the work in [17] is modified by performing the proposed angle extraction in the rotation motion estimation shown in Section. III-A1 after detection on range-Doppler spectra, in order to further improve the angular resolution ability of the original method in that work by introducing Doppler information. Using 3+1D radar, the elevation and azimuth DOA results can be obtained and sent to the algorithm of [17] to get a 3 DoF estimation. This approach will be referred to as '*modified DOA*' method in the rest of the paper and used for comparison. All other state-of-the-art algorithms cannot be implemented without using consecutive frames data, so only the modified DOA algorithm and the proposed algorithm will be compared in this section.

A Hundred Monte Carlo tests were performed, and the error for the 3-dimensional velocity estimation is shown in Fig. 4, and the evaluation results are shown in Table II. As no alternative method can provide the rotational speed estimation based on only one frame, the results of the proposed method are shown in Fig. 5 without comparison.

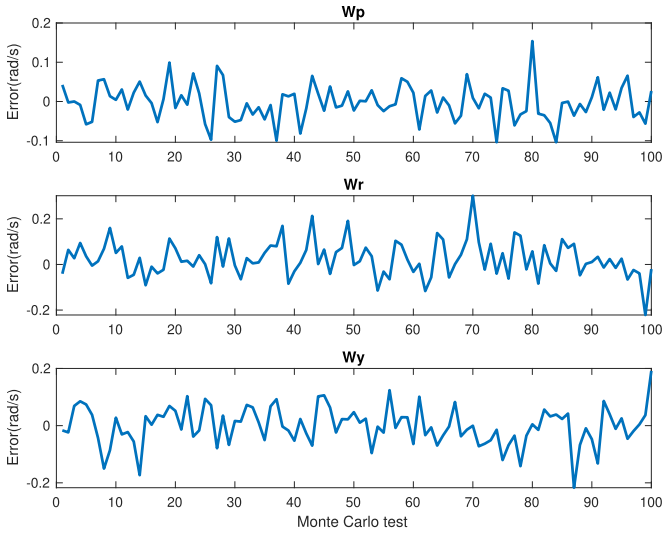

Fig. 5. Performance of the proposed approach in terms of estimation error [rad/s] for 3D rotational velocity for simulated targets. (a) Pitch rotation speed. (b) Roll rotation speed. (c) Yaw rotation speed.

In terms of the estimation of the translational velocity, the proposed curve shown in Fig. 4 is closer to 0 with less fluctuation compared with the Modified DOA method. Also, the proposed method achieves the best performance for every velocity component, with smaller mean error and variance, demonstrating a robust estimation as in Table. II. Regarding the estimation of the rotation velocity in Fig. 5, the error for pitch is 0.0348 rad/s, 0.0609 rad/s for roll and 0.0515 rad/s for yaw. The variance of the error in pitch is 0.002, 0.006 in roll, and 0.0045 in yaw, which is acceptable considering the small values of radar rotation velocity in the ground truth for the simulated scenario.

The performance of the ego-motion estimation will be influenced by the total number of targets in the scene, the ratio of moving targets with respect to the total, and the size of the antenna array. A Hundred additional Monte Carlo tests were performed with respect to each of these parameters to assess their effect while keeping the radar parameters as listed in Table I.

In this new simulation, five hundred targets are placed randomly in the radar field of view. The radar is moving in the three directions with random velocity values. The moving targets' radial velocity follows the uniform distribution $V_r = \mathcal{U}(0, 10.8km/h) = \mathcal{U}(0, 3m/s)$, with varying ratios of moving vs static targets. The SNR is set constant at 20dB. As shown in Table III, the proposed method achieves the best estimation result in all three directions with respect to the mean value and variance of the estimation error. It is expected that with the increase of the moving targets' ratio, the performance drops in all three directions. This is reasonable, as the targets' extra movement will introduce extra Doppler components, and the optimization step in (27) will suffer from this. However, in general, the proposed method is less sensitive to this problem than the alternative method ('modified DOA'). The 'modified DOA' method performs estimation with detected range-Doppler-angle values, instead of exploiting the phase domain, meaning that the extra Doppler velocity induced by targets' random movement will introduce more errors com-

TABLE III

THE EVALUATION RESULTS FOR THE EGO-VELOCITY ESTIMATION'S ERRORS (MEAN AND VARIANCE VALUE IN X Y Z DIRECTION) USING THE SIMULATED POINT TARGETS AS A FUNCTION OF THE RATIO OF MOVING TARGETS

Velocity	Parameters	Methods	Ratio of moving targets 10%	20%	30%	40%	50%	60%
X direction	Mean(m/s)	Modified DOA based	0.1366	0.9086	1.2309	1.4939	1.6131	1.6763
		Proposed	0.0118	0.7721	1.1016	1.3706	1.4860	1.5486
	Variance (10^{-3})	Modified DOA based	1.6	281.5	310.9	423.7	338.0	343.7
		Proposed	0.1	249.3	281.8	400.8	306.8	306.4
Y direction	Mean(m/s)	Modified DOA based	0.0494	0.6841	1.1074	1.4148	1.5805	1.7585
		Proposed	0.0181	0.6733	1.0972	1.4078	1.5794	1.7612
	Variance (10^{-3})	Modified DOA based	1.8	296.6	436.6	364.6	306.9	275.8
		Proposed	0.3	292.8	424.5	342.8	292.9	261.5
Z direction	Mean(m/s)	Modified DOA based	0.0612	0.6861	0.7235	0.8307	0.9579	1.0586
		Proposed	0.0234	0.6705	0.7102	0.8153	0.9436	1.0407
	Variance (10^{-3})	Modified DOA based	2.4	565.4	340.6	360.4	412.2	551.5
		Proposed	0.3	538.3	343.2	332.4	389.7	529.6

pared to the proposed approach. The proposed method uses the least squares solution for solving the optimization problem so that those extra Doppler components will not influence the final result as the majority of targets are still static. Anyhow, as the ratio of moving to static targets increases (e.g., in a dense urban scene with many moving objects), the accuracy of the ego-velocity estimation decreases in the current formulation of the proposed method. A potential solution to this limitation would be to set a threshold separating moving and static targets, and to utilize only those static targets for estimation to avoid the Doppler errors introduced by the targets' own motion.

To test the influence of the array size, another simulation was performed. Five hundred static targets are generated. The radar is moving with random velocities in the 3 directions. The results are shown in Fig. 6. The $Mean_p$ and $Mean_d$ denote the mean error value of the proposed method and the modified DOA method, respectively, while Var_p and Var_d are the error variances of the proposed method and the modified DOA method, respectively. The performance of the proposed methods is marginally improved with a larger array size, as the optimization (27) will highly rely on more data, whereas the performances of the modified DOA method remain almost the same with slight improvement. The estimation of the angle information can be performed with small array sizes because during the detection stage, the targets are separated in the RDS, and the different antenna vectors only provide the information of the differences.

As mentioned in Section. III-D, the number of targets in the scene will influence the detection, and thus the angle estimation within the optimization in (24). On the other hand, if fewer targets are detected, the error will also increase because of the uncertainty. Another Monte Carlo simulation is performed with SNR equal to 20 dB to investigate this aspect with a different overall number of targets in the scene. All the targets are static with the same radar parameters listed in Table I; only the ego-car is moving with random speeds in the three directions. The results are shown in the bar plots of Fig. 7. The proposed method performs consistently better than the modified DOA method. The performance improves at first when more targets are present, and then drops which is

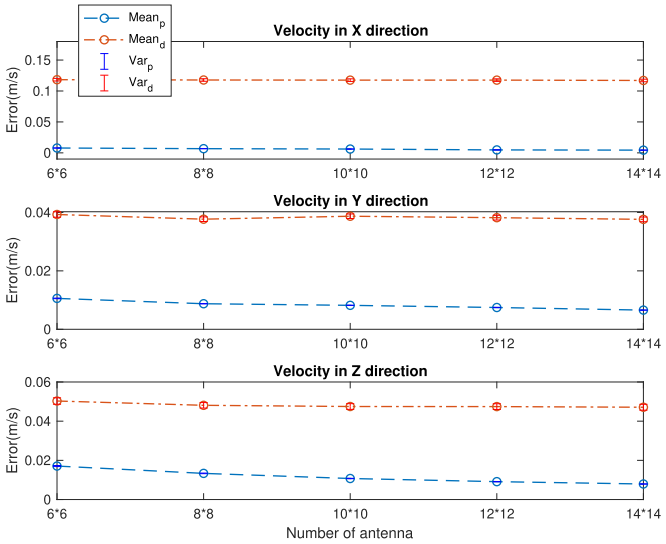

Fig. 6. The error of the velocity estimation in [m/s] with different array sizes. The blue curves refer to the proposed method, whereas the red curves refer to the modified DOA method derived from [17].

visible for both methods as expected. Moreover, one extreme case where 10000 targets are distributed randomly in the scene with the vehicle speed equal to $[18, 54, 7.2]km/h$ was tested. The estimation achieves $0.17km/h$ error in the x-direction, $0.97\ km/h$ in the y-direction and $1.15km/h$ in the z-direction, which is a relatively small proportion compared to the actual speed. This appears to prove that with the current formulation of the algorithm the ego-velocity estimation will be impacted by the presence of many targets, but still provides acceptable performances without failing.

To test the influence of the SNR, another Monte Carlo simulation was performed with values ranging within $[-5, 20]$ dB. There are no obvious differences for different SNRs conditions in terms of the estimation results, hence they are not reported here. This is thought to be related to the fact that the proposed algorithm does not require a certain number of targets detected, but a few static strong targets detected will be sufficient to apply the algorithm. CFAR detection considers the background noise level during its process, so the influence of SNR can be in part compensated. This proves that the algorithm is quite robust to the noise.

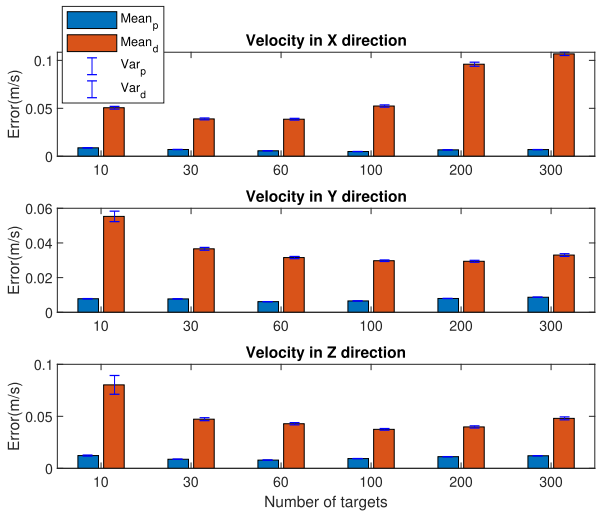

Fig. 7. The error of the velocity estimation in [m/s] with different numbers of static targets. The blue bars refer to the proposed method, whereas the red bars refer to the modified DOA method derived from [17].

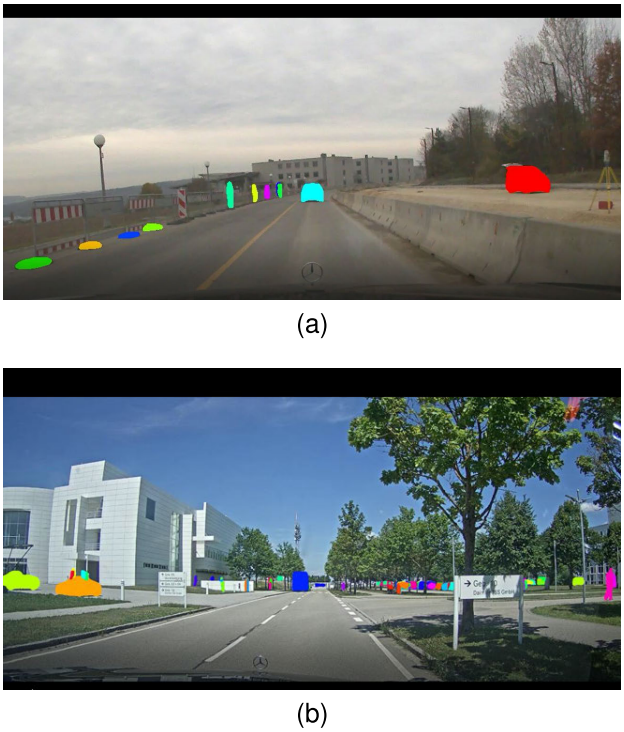

Fig. 8. Pictures of the two experimental automotive scenarios from the dataset (a) Scene1, (b) Scene2.

It is expected from the formulation in section III that if the platform moves faster, the targets will separate more in the range-Doppler spectrum so that their angle estimation will be more accurate. So the effect of this parameter (platform ego-velocity) has not been reported in this subsection. It should also be noted that the velocity components are estimated within one frame with a high update ratio. Nevertheless, the estimation performance could be even improved with the temporal information from past or future frames.

B. Simulated Realistic Scenarios

Two automotive scenarios are generated from the experimental data of the *RadarScenes* [39] dataset to test the proposed algorithm with more realistic data. To generate a scenario with denser targets, all four radars' data from the dataset [39] are used as the source of point scatterers for the simulation. The four radar sensors have a maximum range detection of 100 m and a field of view of about $-60°$ to $+60°$. The range and radial velocity resolution are reported to be 0.15 m and 0.1 km/h, respectively. At the boresight direction, the angular resolution is about 0.5° and degrades to 2° at the outer parts of the field of view. Two scenes are selected to represent two typical automotive scenarios, namely a European city street and a campus road. Two examples of images from the two selected scenes are shown in Fig. 8. As the RadarScenes dataset provides only processed radar point clouds for four radars orientated in different directions, we have used this radar point cloud to synthesise raw data for a single side-looking MIMO radar with 2D uniform antenna array 8×8. The flowchart of the synthesise procedure is shown in Fig. 9. These newly generated raw data have been used for all ego-motion estimation algorithms.

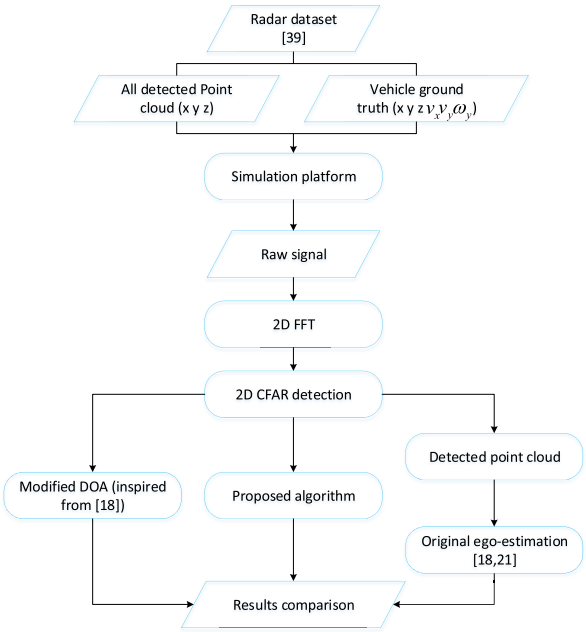

Fig. 9. The comparison flowchart for the proposed method and the modified DOA method implemented on data from the simulated realistic scenarios generated from [39].

To simulate a scene, all the scatter points extracted from the experimental dataset are converted into the world coordinates which are pre-defined in the dataset. As the dataset does not provide height information, all the targets have been set for simplicity at a fixed height of $3m$ for this simulation, and the velocity in the Z direction and the rotation in the X and Y direction are set to 0, as no ground truth is provided for those either. Based on the signal model described in Section II, the corresponding radar signals are generated from the superposition of these scatter points in each frame. Subsequently, the proposed estimation algorithm is used to estimate the ego-velocity.

Two different evaluation metrics are defined to compare different ego-motion estimation algorithms using the simulated realistic data [51]. These are:

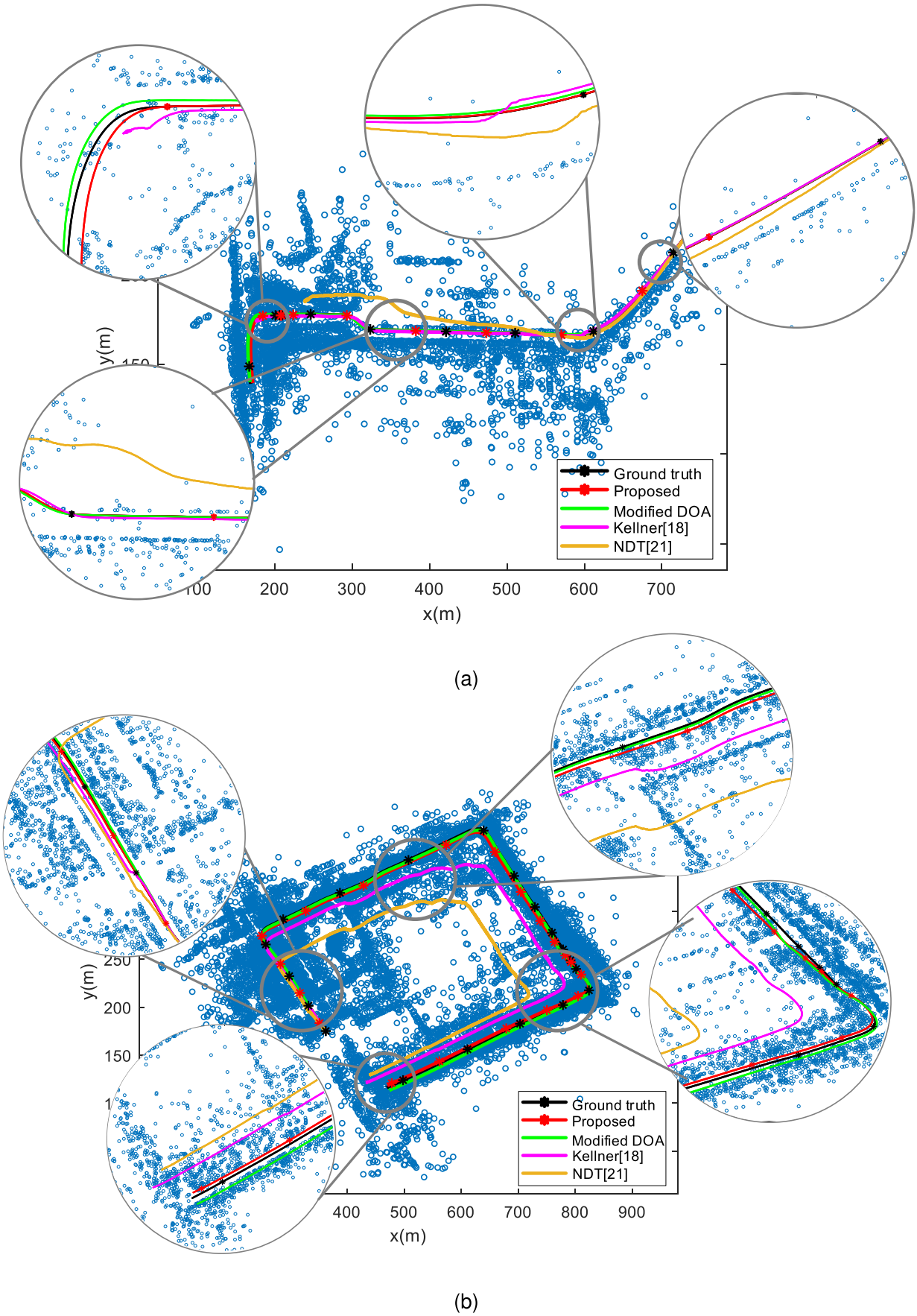

Fig. 10. Estimated trajectory using realistic data from two scenes of [39] with different algorithms (a) Scene1, (b) Scene2.

TABLE IV
THE EVALUATION RESULTS FOR THE TRAJECTORY ESTIMATION (APE, RTE) USING THE REALISTIC DATA FROM TWO SCENES OF [39]

Scene Type	Evaluation metrics		Methods			
			Modified DOA	Proposed	Kellner [12]	NDT [16]
Scene 2	APE(m/s)	Velocity in X direction	0.15	0.11	0.64	1.52
		Velocity in Y direction	0.10	0.10	1.49	1.87
	RTE 100frames(m)		0.10	0.07	0.59	176.56
	RTE 300frames(m)		0.26	0.21	3.43	604

TABLE V
THE EVALUATION RESULTS FOR THE TRAJECTORY ESTIMATION (APE, RTE) USING THE REALISTIC DATA FROM TWO SCENES OF [39]

Scene Type	Evaluation metrics		Methods			
			Modified DOA	Proposed	Kellner [12]	NDT [16]
Scene 1	APE(m/s)	Velocity in X direction	0.09	0.08	0.52	2.26
		Velocity in Y direction	0.06	0.05	1.89	2.02
	RTE 100frames(m)		0.05	0.04	0.44	341.53
	RTE 300frames(m)		0.11	0.10	0.70	1.02e3
Scene 2	APE(m/s)	Velocity in X direction	0.15	0.11	0.64	1.52
		Velocity in Y direction	0.10	0.10	1.49	1.87
	RTE 100frames(m)		0.10	0.07	0.59	176.56
	RTE 300frames(m)		0.26	0.21	3.43	604

1) Absolute Pose Error (APE):

$$\epsilon_{APE} = \sqrt{\frac{1}{m}\sum_{i=1}^{m} \| P_{est}(i) - P_{gro}(i) \|^2} \tag{32}$$

where i is the frame index, m is the total number of frames, P_{est} and P_{gro} are the estimated pose parameters and ground truth poses, respectively.

2) Relative Trajectory Error (RTE): The equation is given in (33), as shown at the top of the next page, where T_{est} and T_{gro} are the estimated trajectory parameters and ground truth trajectory, respectively. N is a relatively short period to evaluate the metric, which is set as 100 and 300 frames in this paper, equivalent to 1.85s and 5.55s, respectively. Essentially, RTE is the average trajectory root-mean-square error (RMSE) over time segments with a length of 100 and 300 frames over which errors can accumulate.

Different ego-motion estimation algorithms have been implemented and compared for these tests, namely: the one by *Kellner* [17] which is the first paper to tackle the ego-motion estimation problem using only radar and achieving a decent and robust performance; the *NDT-based* algorithm in [21] which uses probability and transformation to address the ego-motion estimation problem; the *Modified DOA* algorithm which is the updated version of Kellner's methods as previously explained in this section; and finally the proposed algorithm. For Kellner's method, the number of anchor points is chosen as 100, the probability of inlier ratio is 0.99, and the resulting number of iterations per scan is 10. Regarding the implementation of the selected NDT method, two important hyperparameters of the DBSCAN clustering algorithm [52], the maximum distance and the minimum number of samples, are selected as 2m and 5, respectively.

The resulting vehicle trajectories from these algorithms are shown in Fig.10. All the methods maintain the basic shape of the ground truth trajectory. However, it is clearly shown that the proposed method and the modified DOA method generate estimated trajectories that follow the ground truth almost for the whole duration, while the other two drift or shift to other directions at some points. Both the proposed method and the modified DOA method provide better estimations compared with other alternative methods, based on the evaluation metrics shown in Table IV and Table V. The proposed algorithm provides the smallest error compared with other methods.

V. CONCLUSION

In this paper, a novel algorithm for 3D ego-motion estimation has been proposed, which can operate using only one multi-channel FMCW radar. The proposed algorithm uses the radar raw signals as input and estimates the 3 DoF velocity by estimating first the targets' position and then using their phase information from different times instances. The proposed approach achieves better results compared with algorithms operating on radar point clouds. Starting from raw signals provides opportunities for implementing additional radar signal processing tasks, broadening the limits of alternative SLAM approaches that operate only after several other processing steps used to generate point cloud data.

We verified the proposed algorithm by performing simulations with point-like and realistic scenarios generated from the *RadarScenes* dataset using one side-looking multi-channel FMCW radar. The superior performance of the algorithm in comparison with the state-of-the-art methods is demonstrated. The proposed approach provides very robust results in different scenarios.

Future work will focus on removing the limitations of the current formulation of the proposed method. To address the performance degradation with an increasing ratio of moving to static targets, a possible solution would be introduction of a threshold to distinguish moving vs static targets and only using the static targets' information for ego-velocity estimation. In this way, the computation complexity of the method may also be reduced by considering fewer targets in the optimization stage. To address the potential issue of ambiguous

$$\epsilon_{RTE} = \sqrt{\frac{1}{m-N}\sum_{i=1}^{m-N}(\|T_{est}(i+N) - T_{est}(i)\| - \|T_{gro}(i+N) - T_{gro}(i)\|)^2} \tag{33}$$

velocity values for high speed, FDM, CDM or other Doppler velocity dealiasing techniques [53], [54], [55] to expand the unambiguous velocity range can also be implemented in the processing chain. Finally, to apply the proposed method also in forward-looking radar configuration, the problem of ambiguity in Doppler velocity will need to be solved to help better separate ambiguous targets in individual range-Doppler bins.

ACKNOWLEDGMENT

The authors would like to thank the China Scholarship Council (CSC) for the Ph.D. Scholarship of Sen Yuan.

REFERENCES

[1] R. H. Rasshofer and K. Gresser, "Automotive radar and LiDAR systems for next generation driver assistance functions," *Adv. Radio Sci.*, vol. 3, pp. 205–209, May 2005.

[2] P. Fritsche, B. Zeise, P. Hemme, and B. Wagner, "Fusion of radar, LiDAR and thermal information for hazard detection in low visibility environments," in *Proc. IEEE Int. Symp. Saf., Secur. Rescue Robot. (SSRR)*, Oct. 2017, pp. 96–101.

[3] J. Khalife and Z. M. Kassas, "Differential framework for submeter-accurate vehicular navigation with cellular signals," *IEEE Trans. Intell. Vehicles*, vol. 8, no. 1, pp. 732–744, Jan. 2023.

[4] S. H. Cen and P. Newman, "Precise ego-motion estimation with millimeter-wave radar under diverse and challenging conditions," in *Proc. IEEE Int. Conf. Robot. Autom. (ICRA)*, May 2018, pp. 6045–6052.

[5] F. Engels, P. Heidenreich, A. M. Zoubir, F. K. Jondral, and M. Wintermantel, "Advances in automotive radar: A framework on computationally efficient high-resolution frequency estimation," *IEEE Signal Process. Mag.*, vol. 34, no. 2, pp. 36–46, Mar. 2017.

[6] S. M. Patole, M. Torlak, D. Wang, and M. Ali, "Automotive radars: A review of signal processing techniques," *IEEE Signal Process. Mag.*, vol. 34, no. 2, pp. 22–35, Mar. 2017.

[7] I. Bilik, O. Longman, S. Villeval, and J. Tabrikian, "The rise of radar for autonomous vehicles: Signal processing solutions and future research directions," *IEEE Signal Process. Mag.*, vol. 36, no. 5, pp. 20–31, Sep. 2019.

[8] F. Roos, J. Bechter, C. Knill, B. Schweizer, and C. Waldschmidt, "Radar sensors for autonomous driving: Modulation schemes and interference mitigation," *IEEE Microw. Mag.*, vol. 20, no. 9, pp. 58–72, Sep. 2019.

[9] J. Wang, P. Aubry, and A. Yarovoy, "3-D short-range imaging with irregular MIMO arrays using NUFFT-based range migration algorithm," *IEEE Trans. Geosci. Remote Sens.*, vol. 58, no. 7, pp. 4730–4742, Jul. 2020.

[10] E. Biglieri, R. Calderbank, A. Constantinides, A. Goldsmith, A. Paulraj, and H. V. Poor, *MIMO Wireless Communications*. Cambridge, U.K.: Cambridge Univ. Press, 2007.

[11] Y. Almalioglu, M. Turan, C. X. Lu, N. Trigoni, and A. Markham, "Milli-RIO: Ego-motion estimation with low-cost millimetre-wave radar," *IEEE Sensors J.*, vol. 21, no. 3, pp. 3314–3323, Feb. 2021.

[12] O. Bialer and I. Bilik, "Accurate self localization using automotive radar synthetic aperture radar," U.S. Patent 10 444 347, Oct. 15, 2019.

[13] Y. Li, Y. Liu, Y. Wang, Y. Lin, and W. Shen, "The millimeter-wave radar SLAM assisted by the RCS feature of the target and IMU," *Sensors*, vol. 20, no. 18, p. 5421, Sep. 2020.

[14] A. Kramer, C. Stahoviak, A. Santamaria-Navarro, A.-A. Agha-Mohammadi, and C. Heckman, "Radar-inertial ego-velocity estimation for visually degraded environments," in *Proc. IEEE Int. Conf. Robot. Autom. (ICRA)*, May 2020, pp. 5739–5746.

[15] C. Doer and G. F. Trommer, "Radar visual inertial odometry and radar thermal inertial odometry: Robust navigation even in challenging visual conditions," in *Proc. IEEE/RSJ Int. Conf. Intell. Robots Syst. (IROS)*, Sep. 2021, pp. 331–338.

[16] P. Wallrath and R. Herschel, "Egomotion estimation for a sensor platform by fusion of radar and IMU data," in *Proc. 17th Eur. Radar Conf. (EuRAD)*, Jan. 2021, pp. 314–317.

[17] D. Kellner, M. Barjenbruch, J. Klappstein, J. Dickmann, and K. Dietmayer, "Instantaneous ego-motion estimation using Doppler radar," in *Proc. 16th Int. IEEE Conf. Intell. Transp. Syst. (ITSC)*, Oct. 2013, pp. 869–874.

[18] D. Kellner, M. Barjenbruch, J. Klappstein, J. Dickmann, and K. Dietmayer, "Instantaneous ego-motion estimation using multiple Doppler radars," in *Proc. IEEE Int. Conf. Robot. Autom. (ICRA)*, May 2014, pp. 1592–1597.

[19] M. Barjenbruch, D. Kellner, J. Klappstein, J. Dickmann, and K. Dietmayer, "Joint spatial- and Doppler-based ego-motion estimation for automotive radars," in *Proc. IEEE Intell. Vehicles Symp. (IV)*, Mar. 2015, pp. 839–844.

[20] M. Rapp, M. Barjenbruch, K. Dietmayer, M. Hahn, and J. Dickmann, "A fast probabilistic ego-motion estimation framework for radar," in *Proc. Eur. Conf. Mobile Robots (ECMR)*, Sep. 2015, pp. 1–6.

[21] M. Rapp, M. Barjenbruch, M. Hahn, J. Dickmann, and K. Dietmayer, "Probabilistic ego-motion estimation using multiple automotive radar sensors," *Robot. Auto. Syst.*, vol. 89, pp. 136–146, Mar. 2017.

[22] C. D. Monaco and S. N. Brennan, "RADARODO: Ego-motion estimation from Doppler and spatial data in RADAR images," *IEEE Trans. Intell. Vehicles*, vol. 5, no. 3, pp. 475–484, Sep. 2020.

[23] K. Qian, Z. He, and X. Zhang, "3D point cloud generation with millimeter-wave radar," *Proc. ACM Interact., Mobile, Wearable Ubiquitous Technol.*, vol. 4, no. 4, pp. 1–23, Dec. 2020.

[24] P. Wallrath and R. Herschel, "MIMO radar based platform motion detection for radar imaging," in *Proc. 21st Int. Radar Symp. (IRS)*, Oct. 2020, pp. 351–355.

[25] K. Haggag, S. Lange, T. Pfeifer, and P. Protzel, "A credible and robust approach to ego-motion estimation using an automotive radar," *IEEE Robot. Autom. Lett.*, vol. 7, no. 3, pp. 6020–6027, Jul. 2022.

[26] A. Kingery and D. Song, "Improving ego-velocity estimation of low-cost Doppler radars for vehicles," *IEEE Robot. Autom. Lett.*, vol. 7, no. 4, pp. 9445–9452, Oct. 2022.

[27] M. Magnusson, A. Lilienthal, and T. Duckett, "Scan registration for autonomous mining vehicles using 3D-NDT," *J. Field Robot.*, vol. 24, no. 10, pp. 803–827, 2007.

[28] Y. S. Park, Y.-S. Shin, J. Kim, and A. Kim, "3D ego-motion estimation using low-cost mmWave radars via radar velocity factor for pose-graph SLAM," *IEEE Robot. Autom. Lett.*, vol. 6, no. 4, pp. 7691–7698, Oct. 2021.

[29] S. Lim, J. Jung, S.-C. Kim, and S. Lee, "Radar-based ego-motion estimation of autonomous robot for simultaneous localization and mapping," *IEEE Sensors J.*, vol. 21, no. 19, pp. 21791–21797, Oct. 2021.

[30] H.-W. Cho, S. Choi, Y.-R. Cho, and J. Kim, "Complex-valued channel attention and application in ego-velocity estimation with automotive radar," *IEEE Access*, vol. 9, pp. 17717–17727, 2021.

[31] K. Yeon, K. Min, J. Shin, M. Sunwoo, and M. Han, "Ego-vehicle speed prediction using a long short-term memory based recurrent neural network," *Int. J. Automot. Technol.*, vol. 20, no. 4, pp. 713–722, Aug. 2019.

[32] S. Yuan, F. Fioranelli, and A. Yarovoy, "An approach for high-angular resolution implementation in moving automotive MIMO radar," in *Proc. 18th Eur. Radar Conf. (EuRAD)*, Apr. 2022, pp. 449–452.

[33] S. Yuan, P. Aubry, F. Fioranelli, and A. G. Yarovoy, "A novel approach to unambiguous Doppler beam sharpening for forward-looking MIMO radar," *IEEE Sensors J.*, vol. 22, no. 23, pp. 23494–23506, Dec. 2022.

[34] V. Milanés, S. E. Shladover, J. Spring, C. Nowakowski, H. Kawazoe, and M. Nakamura, "Cooperative adaptive cruise control in real traffic situations," *IEEE Trans. Intell. Transp. Syst.*, vol. 15, no. 1, pp. 296–305, Feb. 2014.

[35] M. Ibarra-Arenado, T. Tjahjadi, J. Pérez-Oria, S. Robla-Gómez, and A. Jiménez-Avello, "Shadow-based vehicle detection in urban traffic," *Sensors*, vol. 17, no. 5, p. 975, Apr. 2017.

[36] B. Zhu, S. Yan, J. Zhao, and W. Deng, "Personalized lane-change assistance system with driver behavior identification," *IEEE Trans. Veh. Technol.*, vol. 67, no. 11, pp. 10293–10306, Nov. 2018.
[37] J. Hasch, "Driving towards 2020: Automotive radar technology trends," in *IEEE MTT-S Int. Microw. Symp. Dig.*, Feb. 2015, pp. 1–4.
[38] M. Gottinger et al., "Coherent automotive radar networks: The next generation of radar-based imaging and mapping," *IEEE J. Microw.*, vol. 1, no. 1, pp. 149–163, Jan. 2021.
[39] O. Schumann et al., "RadarScenes: A real-world radar point cloud data set for automotive applications," in *Proc. IEEE 24th Int. Conf. Inf. Fusion (FUSION)*, Oct. 2021, pp. 1–8.
[40] U. Kumbul, N. Petrov, S. Yuan, C. S. Vaucher, and A. Yarovoy, "MIMO ambiguity functions of different codes with application to phase-coded FMCW radars," in *Proc. Int. Conf. Radar Syst. (RADAR)*, Oct. 2022, pp. 336–341.
[41] A. Farina and F. A. Studer, "A review of CFAR detection techniques in radar systems," *Microw. J.*, vol. 29, no. 9, p. 115, 1987.
[42] C. Chen, C. He, C. Hu, H. Pei, and L. Jiao, "A deep neural network based on an attention mechanism for SAR ship detection in multiscale and complex scenarios," *IEEE Access*, vol. 7, pp. 104848–104863, 2019.
[43] S. Khudoyarov, N. Kim, and J.-J. Lee, "Three-dimensional convolutional neural network–based underground object classification using three-dimensional ground penetrating radar data," *Struct. Health Monitor.*, vol. 19, no. 6, pp. 1884–1893, Nov. 2020.
[44] M. Weiss, "Analysis of some modified cell-averaging CFAR processors in multiple-target situations," *IEEE Trans. Aerosp. Electron. Syst.*, vol. AES-18, no. 1, pp. 102–114, Jan. 1982.
[45] K. S. Arun, T. S. Huang, and S. D. Blostein, "Least-squares fitting of two 3-D point sets," *IEEE Trans. Pattern Anal. Mach. Intell.*, vol. PAMI-9, no. 5, pp. 698–700, Sep. 1987.
[46] W. Kabsch, "A solution for the best rotation to relate two sets of vectors," *Acta Crystallographica Sect. A*, vol. 32, no. 5, pp. 922–923, Sep. 1976.
[47] D. E. Goldberg, *Genetic Algorithms in Search, Optimization and Machine Learning*, 1st ed. Reading, MA, USA: Addison-Wesley, 1989.
[48] S. Kirkpatrick, C. D. Gelatt, and M. P. Vecchi, "Optimization by simulated annealing," *Science*, vol. 220, no. 4598, pp. 671–680, 1983.
[49] C. Audet and J. E. Dennis, "Analysis of generalized pattern searches," *SIAM J. Optim.*, vol. 13, no. 3, pp. 889–903, Jan. 2002.
[50] P. Vasant and N. Barsoum, "Hybrid pattern search and simulated annealing for fuzzy production planning problems," *Comput. Math. Appl.*, vol. 60, no. 4, pp. 1058–1067, Aug. 2010.
[51] R. Giubilato, S. Chiodini, M. Pertile, and S. Debei, "An evaluation of ROS-compatible stereo visual SLAM methods on a nVidia Jetson TX2," *Measurement*, vol. 140, pp. 161–170, Jul. 2019.
[52] M. Ester, H.-P. Kriegel, J. Sander, and X. Xu, "A density-based algorithm for discovering clusters in large spatial databases with noise," in *Proc. KDD*, vol. 96. 1996, pp. 226–231.
[53] T. Tang, C. Wu, and J. Elangage, "A signal processing algorithm of two-phase staggered PRI and slow time signal integration for MTI triangular FMCW multi-target tracking radars," *Sensors*, vol. 21, no. 7, p. 2296, Mar. 2021.
[54] V. Louf, A. Protat, R. C. Jackson, S. M. Collis, and J. Helmus, "UNRAVEL: A robust modular velocity dealiasing technique for Doppler radar," *J. Atmos. Ocean. Technol.*, vol. 37, no. 5, pp. 741–758, May 2020.
[55] M. Wüest, "Dealiasing wind information from Doppler radar for operational use," Ph.D. dissertation, Inst. Atmos. Climate Sci., ETH Zürich, Zürich, Switzerland, 2001.

Sen Yuan (Graduate Student Member, IEEE) was born in Shanxi, China, in 1998. He received the B.E. degree in electronic information engineering and the master's degree in signal processing from Beihang University, Beijing, China, in 2017 and 2020, respectively, with Prof. C. Li and Prof. Z. Yu. He is currently pursuing the Ph.D. degree in microwave sensing signals and systems with the Department of Microelectronics, Delft University of Technology (TU Delft), Delft, The Netherlands.

In 2016, he did an Internship with Tsinghua University, Beijing, about navigation with Dr. X. Chen. During his graduate education, he studied and became familiar with the SAR, including its satellite orbits, system design, and ground processing. In January 2021, he joined TU Delft, where he works on millimeter radar signal processing in automotive applications.

Simin Zhu (Graduate Student Member, IEEE) received the B.Sc. degree in electrical engineering and automation from Central South University in 2016, and the master's degree in radar signal processing and machine learning from the Microwave Sensing, Signals and Systems (MS3) Group, Delft University of Technology (TU Delft), in November 2021, where he is currently pursuing the Ph.D. degree. After graduation, he worked for 1.5 years as a Hardware Engineer at Huawei Technology Company Ltd.

Francesco Fioranelli (Senior Member, IEEE) received the Laurea (B.Eng., cum laude) and Laurea Specialistica (M.Eng., cum laude) degrees in telecommunication engineering from Università Politecnica delle Marche, Ancona, Italy, in 2007 and 2010, respectively, and the Ph.D. degree from Durham University, U.K., in 2014.

He was an Assistant Professor with the University of Glasgow from 2016 to 2019 and a Research Associate with University College London from 2014 to 2016. He is currently an Associate Professor with the Delft University of Technology (TU Delft), The Netherlands. He has authored over 140 publications between book chapters, journal and conference papers, edited the books on "micro-doppler radar and its applications" and "radar countermeasures for unmanned aerial vehicles" published by IET-Scitech in 2020. His research interests include the development of radar systems and automatic classification for human signatures analysis in healthcare and security, drones and UAVs detection and classification, automotive radar, wind farm, and sea clutter. He received three best paper awards.

Alexander G. Yarovoy (Fellow, IEEE) received the Diploma degree (Hons.) in radiophysics and electronics from Kharkov State University, Kharkiv, Ukraine, in 1984, and the Candidate Physics and Mathematical Sciences and Doctor Physics and Mathematical Sciences degrees in radiophysics, in 1987 and 1994, respectively.

In 1987, he joined the Department of Radiophysics, Kharkov State University, as a Researcher and became a Full Professor in 1997. From September 1994 to 1996, he was with the Technical University of Ilmenau, Germany, as a Visiting Researcher. Since 1999, he has been with the Delft University of Technology, The Netherlands, where he has been leading as the Chair of the Microwave Sensing, Systems and Signals Group since 2009. He has authored and coauthored more than 500 scientific or technical articles, seven patents, and 14 book chapters. His main research interests are in high-resolution radar, microwave imaging, and applied electromagnetics (in particular, UWB antennas).

Prof. Yarovoy was a recipient of the European Microwave Week Radar Award for the paper that best advances the state-of-the-art in radar technology in 2001 (together with L. P. Ligthart and P. van Genderen) and in 2012 (together with T. Savelyev). In 2010 together with D. Caratelli, he got the Best Paper Award of the Applied Computational Electromagnetic Society (ACES). He served as the General TPC Chair for the 2020 European Microwave Week (EuMW'20), as the Chair and the TPC Chair for the 5th European Radar Conference (EuRAD'08), and a Secretary for the 1st European Radar Conference (EuRAD'04). He also served as the Co-Chair and the TPC Chair for the Xth International Conference on GPR (GPR2004). From 2011 to 2018, he served as an Associate Editor for the *International Journal of Microwave and Wireless Technologies*. He serves as an Associate Editor for the IEEE TRANSACTION ON RADAR SYSTEMS. From 2008 to 2017, he served as the Director of the European Microwave Association (EuMA).